

# Nanoscale

Accepted Manuscript



This is an *Accepted Manuscript*, which has been through the Royal Society of Chemistry peer review process and has been accepted for publication.

*Accepted Manuscripts* are published online shortly after acceptance, before technical editing, formatting and proof reading. Using this free service, authors can make their results available to the community, in citable form, before we publish the edited article. We will replace this *Accepted Manuscript* with the edited and formatted *Advance Article* as soon as it is available.

You can find more information about *Accepted Manuscripts* in the [Information for Authors](#).

Please note that technical editing may introduce minor changes to the text and/or graphics, which may alter content. The journal's standard [Terms & Conditions](#) and the [Ethical guidelines](#) still apply. In no event shall the Royal Society of Chemistry be held responsible for any errors or omissions in this *Accepted Manuscript* or any consequences arising from the use of any information it contains.

**Stable, high-responsive and broadband photodetection based on large-area  
multilayer WS<sub>2</sub> films grown by pulsed-laser deposition**

J. D. Yao, Z. Q. Zheng, J. M. Shao & G. W. Yang \*

State Key Laboratory of Optoelectronic Materials and Technologies, Nanotechnology  
Research Center, School of Physics & Engineering, Sun Yat-sen University,  
Guangzhou 510275, Guangdong, P. R. China

\*Corresponding author: [stsygw@mail.sysu.edu.cn](mailto:stsygw@mail.sysu.edu.cn)

### Abstract

The progress of graphene has aroused the renaissance of keen research interests on the layered transition metal dichalcogenides (TMDs). Tungsten disulfide ( $\text{WS}_2$ ), a typical TMD with favorable semiconducting band gap and strong light-matter interaction, exhibits great potential in high-responsive photodetection. However,  $\text{WS}_2$ -based photodetection is currently unsatisfactory due to the low optical absorption (2%-10%) and poor carrier mobility ( $0.01\text{-}0.91\text{ cm}^2\text{V}^{-1}\text{s}^{-1}$ ) of the thin  $\text{WS}_2$  layers grown by chemical vapor deposition (CVD). Here, we introduce pulsed-laser deposition (PLD) to prepare the multilayer  $\text{WS}_2$  films. Large-area  $\text{WS}_2$  films at the magnitude of  $\text{cm}^2$  are achieved. Comparative measurements of a  $\text{WS}_2$ -based photoresistor demonstrate its stable broadband photoresponse from 370 to 1064 nm, the broadest range demonstrated in  $\text{WS}_2$  photodetectors. Benefit from the large optical absorbance (40%-85 %) and high carries mobility ( $31\text{ cm}^2\text{V}^{-1}\text{s}^{-1}$ ), the responsivity of the device approaches a high value of 0.51 A/W in the ambient environment. Such a performance far surpasses the CVD-grown  $\text{WS}_2$ -based photodetectors ( $\mu\text{A}/\text{W}$ ). In the vacuum environment, the responsivity is further enhanced to 0.70 A/W along with an external quantum efficiency of 137% and a photodetectivity of  $2.7 \times 10^9\text{ cm} \cdot \text{Hz}^{1/2} \cdot \text{W}^{-1}$ . These findings stress that the PLD-grown  $\text{WS}_2$  film may constitute a new paradigm for the next-generation stable, broadband and high-responsive photodetectors.

## Introduction

Over the past few years, transition metal dichalcogenides (TMDs) have made significant steps forward in the field of photodetection owing to their strong light-matter interaction and favorable semiconducting band gaps ( $1 \sim 2$  eV).<sup>1, 2</sup> In general, they are a family of layered materials consist of stacked covalently bonded X-M-X (M = Mo, W, Nb, Ta, Ti, Re and S = S, Se, Te) molecular layers held together via weak van der Waals interactions. Among the family of TMDs, molybdenum disulfide (MoS<sub>2</sub>) is the representative and has undergone the most extensive researches. The first monolayer-MoS<sub>2</sub> based phototransistor exhibits fast response time within 50 ms and shows good stability.<sup>3</sup> However, it suffers low responsivity of 7 mA/W due to its low optical absorbance and poor carrier mobility of  $0.11 \text{ cm}^2V^{-1}s^{-1}$ .<sup>3</sup> Later, benefit from the increase of optical absorbance, multilayer-MoS<sub>2</sub> based photodetectors demonstrated their superiority with the responsivity more than one magnitude higher, from 100 to 570 mA/W.<sup>4, 5</sup> Besides, due to the relatively weak confinement effect, the multilayer-MoS<sub>2</sub> based device offers a broader response spectral from visible to near-infrared, which can be superior to their monolayer/few-layer counterparts in multifunctional applications.<sup>4, 5</sup>

Tungsten disulfide (WS<sub>2</sub>), another typical member among the TMD group, has proven wider working temperature range than other TMD materials, suggesting superior thermal stability for widespread application.<sup>6</sup> Meanwhile, theoretical calculation has pointed out that WS<sub>2</sub> enjoys a smaller electron effective mass and thus have a higher carrier mobility.<sup>7</sup> Consequently, there are many attractive potential

opportunities for WS<sub>2</sub>-based photodetectors. However, to date, attempts on WS<sub>2</sub> photodetectors are scarce. Photodetectors based on mechanical exfoliated WS<sub>2</sub> nanosheets exhibits high responsivity from 0.1 A/W to 5.7 A/W.<sup>8-11</sup> Nevertheless, they suffer the predicament in practical device implement because the lateral dimensions of the exfoliated flakes are mostly limited to hundreds of micrometers, not to mention the randomness of the shape, thickness and crystal quality. Electronic-grade WS<sub>2</sub> films, which are essential for imaging pixels and display applications requiring large arrays of photodetectors, are unattainable due to the uncontrollability and low efficiency of the mechanical exfoliation method. Recently, chemical vapor deposition (CVD) was developed to successfully obtain large-area WS<sub>2</sub> flacks.<sup>12</sup> However, the yield of CVD is so low that the CVD-grown WS<sub>2</sub> samples are usually monolayer or few-layer instead of the preferable multilayer, which seriously limits their optical absorbance. On the other hand, the CVD-grown WS<sub>2</sub> layers usually suffer low carrier mobility from 0.01 to 0.91  $cm^2V^{-1}s^{-1}$  due to the serious scattering. Such scattering is probably induced by the external environment, e.g. the adsorbate at the top surface, the phonons generated by the vibration of the adsorbate and the trapped defects induced by the SiO<sub>2</sub> at the bottom surface.<sup>3,13</sup> Consequently, photodetectors based on them exhibit low responsivity at the magnitude of  $\sim \mu A/W$  even with the help of a large electric field.<sup>14, 15</sup> So far, high-responsive WS<sub>2</sub> photodetectors based on high-efficient, large-area deposition techniques have not been reported yet. Consequently, there is an emerging demand for an alternative deposition technology for large-area WS<sub>2</sub> films.

Pulse laser deposition (PLD) is a facile and scalable deposition technique which can reproduce the components of the target precisely onto the substrate.<sup>16, 17</sup> Unlike CVD and molecular beam epitaxy (MBE), it is easy to operate and holds the advantages of high efficiency, while the cost is low. Recently, high-quality PLD-grown MoS<sub>2</sub> films and GaSe nanosheets networks for photodetection application were developed.<sup>18, 19</sup> Considering the great applicability of PLD, it is tempting to exploit it to prepare large-area WS<sub>2</sub> films and develop their possibility for high-responsive broadband photodetection.

Here, we introduced PLD to prepare multilayer WS<sub>2</sub> films. Interestingly, high-quality, large-area multilayer WS<sub>2</sub> films were prepared. Meanwhile, a photoresistor-like device was constructed by patterning two Pt electrodes at two opposite sides of the PLD-grown WS<sub>2</sub> film (Supplementary information S1) and the photoresponse was characterized systematically. Comparative measurements demonstrate its stable broadband photoresponse from 370 to 1064 nm with good reproducibility. The photoresponsivity approaches 0.51 A/W in the air environment. Besides, the photocurrent exhibits positive dependence on both the source-drain voltage and the incident power, offering good tunability for multi-purpose applications. In the vacuum environment, the responsivity of the device is further enhanced to 0.7 A/W along with an external quantum efficiency of 137% and a photodetectivity of  $2.7 \times 10^9 \text{ cm} \cdot \text{Hz}^{1/2} \cdot \text{W}^{-1}$ . Therefore, these results demonstrate a promising methodology for the development of TMD material in the future.

## Experiment

PLD was exploited to prepare the WS<sub>2</sub> thin films. In our experiment, the deposition parameters are as follows. The base pressure of the growth chamber is better than  $1 \times 10^{-4}$  Pa. The target is consisted of stoichiometric W (99.9%) and S (99.9%) elements with the W: S atomic ratio of 1: 2. Prior to loading into the growth chamber, the substrates were washed following a standard cleaning procedure to obtain a clean surface. Pre-growth annealing at 500° C for 30 minutes was performed to remove the native contaminations from the substrate. Large-area WS<sub>2</sub> films were deposited at the optimized substrate temperature of 500° C, and the working pressure was set at 50 Pa with flowing Ar<sub>2</sub> as the working gas in the rate of 50 sccm.

Illuminations with wavelength of 370, 532, 635 and 1064 nm were generated from the semiconductor lasers. The transport characteristics of the WS<sub>2</sub> photoresistor were evaluated using a Keithley 4200-SCS semiconductor parameter analyzer equipped with a probe station. All measurements were performed at room temperature under ambient condition unless specially noted.

## Results and Discussion

Fig. 1 (a) presents a digital photograph of a PLD-grown multilayer WS<sub>2</sub> film on a Si substrate with a 300 nm thermally grown oxide layer. To get a shape contrast, the substrate is partly covered with a stainless steel mask during the growth process. As can be seen, the uncovered area all appears in light green color while the covered area remains purple, indicating the growth of WS<sub>2</sub>. Hence, a large-area WS<sub>2</sub> film with the lateral size at the magnitude of one centimeter is achieved. Scalable WS<sub>2</sub> film can be readily obtained by just changing the size of the substrate. Compared to quantum dots

and nanowires, films are more compatible and easier to be fabricated into various complex integrated structures with the state-of-art thin film micromanufacturing techniques. Thus, such result is of great significance to practical device implement. Then, scanning electron microscope (SEM), atomic force microscopy (AFM), energy dispersive spectroscopy (EDS), X-ray diffraction (XRD) and Raman spectroscopy were conducted to access the morphology, constituent, crystalline quality and structure of the PLD-grown WS<sub>2</sub> film. Fig. 1(b) presents a typical SEM image, showing continuous polycrystalline morphology. The corresponding EDS result (Supplementary information S2, Fig. S2(a)) presents only the peaks of W and S, suggesting high purity of the PLD-grown WS<sub>2</sub> film. The component analysis (Supplementary information S2, Fig. S2(b)) shows the stoichiometry W to S atomic ratio of ~ 1:2. Then, the AFM surface topography image is shown in Fig. 1(c). The surface of the WS<sub>2</sub> film is found to be quiet smooth with a RMS of c.a. 1.8 nm. The thickness of the film is measured by the AFM thickness profile. Specimen for the thickness measurement was prepared by scratching the film using a blade. It is found that the thickness is c.a. 60 nm (Supplementary information S2, Fig. S2(c)). The XRD pattern of the sample is presented in Fig. 1(d). There is only one prominent peak indexed as (002), suggesting highly oriented property of the film. To further access the crystal structure, Raman scattering measurement with the 514 nm excitation laser was conducted, as shown in Fig. 1(e). There are three main peaks at 175, 356.5 and 420.6 cm<sup>-1</sup>, assigned respectively as the first order Raman modes LA(M), E<sub>2g</sub><sup>1</sup> and A<sub>1g</sub>. There are also other weaker peaks corresponding to the second order Raman

modes, which are marked in the labels. Our Raman spectroscopy agrees well with that of previous results obtained from the CVD-synthesised and mechanically-exfoliated samples.<sup>8, 14</sup> Generally, the above-mentioned systematic characterizations indicate that the PLD-grown WS<sub>2</sub> film is of good quality and offers an attractive material platform to develop opportunities hidden in WS<sub>2</sub>.

Fig. 2(a) depicts the optical absorption spectrum of the PLD-grown WS<sub>2</sub> film. Compared to the monolayer/few-layer counterparts, whose absorption spectrum cuts off at a relatively short wavelength of c.a. 700 nm,<sup>20</sup> the multilayer WS<sub>2</sub> film enjoys a much broader absorbance range covering from the ultraviolet to the near-infrared. The broadening of the absorption range is benefit from the weakened confinement effect of the multilayer WS<sub>2</sub>. As depicted in the inset of Fig. 2(a), for the monolayer WS<sub>2</sub>, only the direct excitation corresponding to a large bandgap is allowed. When the film grows to multilayer, the indirect excitation corresponding to a smaller band gap is also allowed, thus leading to the broadening of the absorption range.<sup>21</sup> Besides, the interfacial state in the grain boundaries and defects may constitute an impurity band residing inside the band gap, which may further extend the absorption edge to a longer wavelength. On account of the increase of the optical active layers, the absorption rate of the multilayer WS<sub>2</sub> exceeds 40 % over the whole measured range with the absorption peak of 85 % at c.a. 700 nm, far exceeding the value of 2 % ~ 10 % reported for monolayer WS<sub>2</sub>.<sup>22, 23</sup> The appearance of the absorption peak at c.a. 700 nm is probably due to the stronger light matter interaction at a wavelength matching the band gap of the monolayer/few-layer WS<sub>2</sub>.

The mobility of the PLD-grown films is measured by the Hall system and the corresponding distribution histogram for nine samples is summarized in Fig. 2(b). The average mobility is calculated to be  $31 \text{ cm}^2 \text{ V}^{-1} \text{ s}^{-1}$ , far surpassing the value of the CVD-grown flakes from  $0.01 \sim 0.91 \text{ cm}^2 \text{ V}^{-1} \text{ s}^{-1}$ .<sup>12, 24, 25</sup> The reason for the higher mobility is the relatively weaker scattering of a thicker sample. For the multilayer sample, the surface-to-volume ratio is relatively small. That is, surface channel only counts a little portion of the total transport. Therefore, contrary to the monolayer/few-layer case, the degradation effects of the external-environment induced scattering on the total transport are negligible. Finally, the cross-sectional view of a typical WS<sub>2</sub> photoresistor is delineated in Fig. 2(c). The device is consisted of a PLD-grown WS<sub>2</sub> film and two Pt electrodes, manufactured onto a Si wafer with a 300 nm-thick SiO<sub>2</sub> dielectric layer to avoid the interference of the substrate channel on the transport measurements, ensuring that the response comes from the WS<sub>2</sub>. Fig. 3 presents the switching behavior of the WS<sub>2</sub> photoresistor under a periodic illumination with different laser wavelengths from the ultraviolet to the near-infrared, including (a) 370, (b) 532, (c) 635 and (d) 1064 nm. In all illumination cases, the device yields a significant photocurrent and exhibits a good reproducibility during all on-off cycles, demonstrating the feasibility for broadband photodetection. As far as we know, this is the broadest responsive range reported for WS<sub>2</sub> hitherto.

To have a further insight into the WS<sub>2</sub> photodetector, the response time, the influences of the incident light intensity and the source-drain voltage on the device performance as well as the air stability were investigated. As shown in Fig. 4(a), on

light illumination, the photocurrent rises to a high level state quickly at the beginning, followed by a relatively slow tail. A reversed behavior is observed when the light is turned off. The rise and decay time (the time needed to change by 90%) extracted from the temporal response curve are 4.1 s and 4.4 s, respectively. Fig. 4(b) presents the power dependent photocurrent, the photocurrent increase with the increase of incident light intensity, due to the increase of photogenerated carriers. The data are fitted by the power law  $I = AP^n$  and the  $n$  is extracted to be 0.87, indicating a near linear relationship. Fig. 4(c) presents the voltage dependent photocurrent and the corresponding responsivity. The responsivity  $R$  of the device is calculated by  $R = \frac{I_p}{P \times S}$ , where  $I_p$  is the photocurrent,  $P$  is the power density and  $S$  is the active area. The photocurrent increases with the voltage, benefit from the increased separation efficiency of photogenerated carriers and enhancement of impact ionization. The responsivity of the device under a 635 nm illumination with a source-drain voltage of 9 V reaches a decent value of 0.51 A/W. Such responsivity is comparable to the exfoliated WS<sub>2</sub> based devices and several orders of magnitude larger than that of the CVD-grown samples, e.g.  $2.5 \times 10^6$  times of that of monolayer WS<sub>2</sub> and  $5.5 \times 10^3$  times of that of few layer WS<sub>2</sub> (Supplementary information S3). As far as we know, this is the largest value reported for a WS<sub>2</sub> photodetector based on a large-area deposition technique.

The corresponding  $EQE = \frac{hcR}{e\lambda}$ , where  $h$  is the Planck constant,  $c$  is the light speed,  $e$  is the elementary charge and  $\lambda$  is the wavelength, is calculated to be 101%.

And the detectivity  $D^* = A^{1/2}R / (2eI_d)^{1/2}$ ,  $I_d$  is the dark current and  $A$  is the active area,

is calculated to be  $1.93 \times 10^9 \text{ cm} \cdot \text{Hz}^{1/2} \cdot \text{W}^{-1}$ . Such a decent device performance can be attributed to the higher mobility and absorption of our multilayer  $\text{WS}_2$  film. Generally, on light illumination, the photocurrent can be expressed as  $I_p \propto \alpha \mu \tau$ , where  $\alpha$  is the absorption of incident light,  $\mu$  is the carrier mobility and  $\tau$  is the carrier lifetime. Compared to the monolayer and few layer  $\text{WS}_2$ , the PLD-grown multilayer  $\text{WS}_2$  enjoys a higher light absorption rate  $\alpha$ . Besides, they are demonstrated to possess higher mobility  $\mu$  than that of the CVD-grown thin  $\text{WS}_2$  layers. Consequently, the alliance of such two advantages results in excellent device performance. Additionally, the endurance of the device to the air environment is evaluated. The device was placed in the air without sealed encapsulation for a month and then its photoresponse was evaluated, as depicted in Fig. 4(d). Excitingly, the device still enjoys definite switching behavior with good reproducibility. Such high stability is originated from the excellent chemical stability of  $\text{WS}_2$ , suggesting great potential to widespread commercial photodetectors.

Considering that TMDs are excellent gas-sensing materials,<sup>26</sup> the effects of chemisorptions on the photoresponse of the PLD-grown multilayer  $\text{WS}_2$  based photoresistor were explored. Firstly, the photoresponse of the  $\text{WS}_2$  photoresistor to a cyclical light illumination under vacuum environment is presented in Fig. 5(a). The device exhibits definite switching behavior, demonstrating good reproducibility in the vacuum environment. Fig. 5(b) presents the power dependent photocurrent, the photocurrent also increase with the increase of the incident light intensity. The data are fitted by the power law  $I = AP^n$  and the  $n$  is extracted to be 0.88, indicating a

near linear relationship. Fig. 5(c) depicts the voltage dependent photocurrent and the corresponding responsivity. The photocurrent also increases with the increase of source-drain voltage. For comparison, the voltage dependent photocurrent in air (black dash line) is also plotted in Fig. 5(c). As can be seen, the photocurrent in the vacuum environment is larger than that in air. Such enhancement of the photocurrent in the vacuum indicates great potential in aerial photodetection. The responsivity of the device under a 635 nm illumination with a source-drain voltage of 9 V reaches a decent value of 0.7 A/W, with the corresponding EQE of 137% and detectivity of  $2.7 \times 10^9 \text{ cm} \cdot \text{Hz}^{1/2} \cdot \text{W}^{-1}$ . Fig. 5(d) presents the temporal response of the photodetector in vacuum. The rise and decay times in vacuum are 9.9 s and 8.7 s, slower than that of 4.1 s and 4.4 s in air. More than 10 devices have been produced and similar results were duplicated. All of the above results indicate that the atmosphere environment has a great influence on the device performance.

Then, the mechanism underneath the enhancement of the responsivity of the WS<sub>2</sub> photodetector in the vacuum environment is investigated. The air is consisted of 78 % N<sub>2</sub>, 21 % O<sub>2</sub> and 1 % of the rest. Considering that the N<sub>2</sub> is an inactive gas, the influence of the air can thus be mainly attributed to the O<sub>2</sub>. As is well known, O<sub>2</sub> molecules are active electron acceptors.<sup>27</sup> Therefore, the WS<sub>2</sub> film tends to absorb a large number of O<sub>2</sub> molecules when it is transferred into the ambient environment. As depicted schematically in Fig. 5(f), the absorption of O<sub>2</sub> will lead to the consumption of electrons



On the other hand, the  $O_2^-$  can combine with a hole and escape back to the air



The combination of the adsorption and desorption processes equals to the recombination of the electron-hole pairs, i.e.  $O_2^-$  acts as recombination centers for the photogenerated carriers. Therefore, the more the number of adsorbed  $O_2$  molecules, the easier the recombination of the photogenerated carriers, that is, the shorter of the carrier life  $\tau$ . In the vacuum environment, the rarefied atmosphere leads to the less adsorbate and thus less recombination centers. Considering that the response time of the device is usually negatively correlated with the life time of the photogenerated carriers, the response time in the vacuum should be longer than that in the ambient, which is in good agreement of our experimental results.

Another possible reason for the difference of the photoresponse between air and vacuum is the change of the carrier mobility induced by the adsorbate. Note that the absorption of  $O_2$  also induces negatively charged impurities on the surface in concentrations of the adsorbate. Besides, the oscillation of the adsorbate may further introduce the local phonons. As a result, the scattering of the carriers is enhanced and therefore the mobility  $\mu$  of the film decreases.<sup>13</sup> However, unlike the monolayer/few-layer cases, for the multilayer sample, the surface channel only accounts for a little portion of the total transportation. Consequently, the influence of the adsorbate on the transport of the multilayer sample should be weak. Fig. 5(e) presents the I-V curves in the ambient (dark curve) and vacuum environments (red curve), respectively. The two curves exhibit almost the same slope, suggesting the

same mobility in both environments. Consequently, the mobility of the PLD-grown multilayer WS<sub>2</sub> film is insensitive to the environmental factors. Given that the photocurrent can be expressed as  $I_p \propto \alpha \mu \tau$ . Therefore, the larger photocurrent in the vacuum condition should be attributed to its longer carrier life time considering the same absorbance and mobility.

### Conclusion

In summary, we have exploited PLD to deposit the multilayer WS<sub>2</sub> films and explored its photoresponse. The fabricated device showed stable broadband photoresponse with a good reproducibility. The photoresponse in air reaches 0.51 A/W, several orders of magnitude larger than that of the CVD-grown monolayer and multilayer WS<sub>2</sub> film. In the vacuum environment, the photoresponse can be enhanced to 0.7 A/W. Our studies also showed that the performance of the device may be further improved by appropriate strategies, e.g. optimizing the contacts,<sup>28</sup> plasmonic enhancement of optical absorbance,<sup>29</sup> tailing the electronic structure by doping or surface modification<sup>30</sup> and constructing a heterojunction with newly emerging wide band gap material.<sup>31</sup> These results evidenced that PLD offers a convenient mean for large-area WS<sub>2</sub> films. Consequently, the scheme for practical high-responsive broadband WS<sub>2</sub> photodetectors may be actualized in the near future.

### Acknowledgements

The National Basic Research Program of China (2014CB931700) and State Key Laboratory of Optoelectronic Materials and Technologies supported this work.

## References

1. Q. H. Wang, K. Kalantar-Zadeh, A. Kis, J. N. Coleman and M. S. Strano, *Nat Nano*, 2012, **7**, 699-712.
2. D. Jariwala, V. K. Sangwan, L. J. Lauhon, T. J. Marks and M. C. Hersam, *ACS nano*, 2014, **8**, 1102-1120.
3. Z. Yin, H. Li, H. Li, L. Jiang, Y. Shi, Y. Sun, G. Lu, Q. Zhang, X. Chen and H. Zhang, *ACS Nano*, 2011, **6**, 74-80.
4. W. Choi, M. Y. Cho, A. Konar, J. H. Lee, G. B. Cha, S. C. Hong, S. Kim, J. Kim, D. Jena and J. Joo, *Adv Mater*, 2012, **24**, 5832-5836.
5. D.-S. Tsai, K.-K. Liu, D.-H. Lien, M.-L. Tsai, C.-F. Kang, C.-A. Lin, L.-J. Li and J.-H. He, *Acs Nano*, 2013, **7**, 3905-3911.
6. W. A. Brainard, 1969.
7. L. Liu, S. Bala Kumar, Y. Ouyang and J. Guo, *Electron Devices, IEEE Transactions on*, 2011, **58**, 3042-3047.
8. N. Huo, S. Yang, Z. Wei, S.-S. Li, J.-B. Xia and J. Li, *Scientific reports*, 2014, **4**.
9. S. Hwan Lee, D. Lee, W. Sik Hwang, E. Hwang, D. Jena and W. Jong Yoo, *Appl Phys Lett*, 2014, **104**, 193113.
10. L. Britnell, R. Ribeiro, A. Eckmann, R. Jalil, B. Belle, A. Mishchenko, Y.-J. Kim, R. Gorbachev, T. Georgiou and S. Morozov, *Science*, 2013, **340**, 1311-1314.
11. N. Huo, J. Kang, Z. Wei, S. S. Li, J. Li and S. H. Wei, *Adv Funct Mater*, 2014, **24**, 7025-7031.
12. A. L. Elías, N. Perea-López, A. Castro-Beltrán, A. Berkdemir, R. Lv, S. Feng, A.

- D. Long, T. Hayashi, Y. A. Kim and M. Endo, *ACS nano*, 2013, **7**, 5235-5242.
13. G. Sumanasekera, C. Adu, S. Fang and P. Eklund, *Phys Rev Lett*, 2000, **85**, 1096.
14. N. yPerea-López, A. L. Elías, A. Berkdemir, A. Castro-Beltran, H. R. Gutiérrez, S. Feng, R. Lv, T. Hayashi, F. López-Urías, S. Ghosh, B. Muchharla, S. Talapatra, H. Terrones and M. Terrones, *Adv Funct Mater*, 2013, **23**, 5511-5517.
15. C. Lan, C. Li, Y. Yin and Y. Liu, *Nanoscale*, 2015.
16. J. Yao, J. Shao, Y. Wang, Z. Zhao and G. Yang, *Nanoscale*, 2015.
17. H. Zhang, J. Yao, J. Shao, H. Li, S. Li, D. Bao, C. Wang and G. Yang, *Scientific reports*, 2014, **4**, 5876.
18. M. Mahjouri - Samani, R. Gresback, M. Tian, K. Wang, A. A. Puretzky, C. M. Rouleau, G. Eres, I. N. Ivanov, K. Xiao and M. A. McGuire, *Adv Funct Mater*, 2014, **24**, 6365-6371.
19. D. J. Late, P. A. Shaikh, R. Khare, R. V. Kashid, M. Chaudhary, M. A. More and S. B. Ogale, *ACS applied materials & interfaces*, 2014, **6**, 15881-15888.
20. M. Shanmugam, C. A. Durcan, R. Jacobs-Gedrim and B. Yu, *Nano Energy*, 2013, **2**, 419-424.
21. W. S. Yun, S. Han, S. C. Hong, I. G. Kim and J. Lee, *Phys Rev B*, 2012, **85**, 033305.
22. M. Bernardi, M. Palummo and J. C. Grossman, *Nano letters*, 2013, **13**, 3664-3670.
23. Y. Yu, S. Hu, L. Su, L. Huang, Y. Liu, Z. Jin, A. A. Purezky, D. B. Geohegan, K.

- W. Kim, Y. Zhang and L. Cao, *Nano letters*, 2015, **15**, 486-491.
24. Y. Zhang, Y. Zhang, Q. Ji, J. Ju, H. Yuan, J. Shi, T. Gao, D. Ma, M. Liu, Y. Chen, X. Song, H. Y. Hwang, Y. Cui and Z. Liu, *ACS Nano*, 2013, **7**, 8963-8971.
25. Y.-H. Lee, L. Yu, H. Wang, W. Fang, X. Ling, Y. Shi, C.-T. Lin, J.-K. Huang, M.-T. Chang, C.-S. Chang, M. Dresselhaus, T. Palacios, L.-J. Li and J. Kong, *Nano letters*, 2013, **13**, 1852-1857.
26. K. Lee, R. Gatensby, N. McEvoy, T. Hallam and G. S. Duesberg, *Adv Mater*, 2013, **25**, 6699-6702.
27. S.-W. Fan, A. K. Srivastava and V. P. Dravid, *Appl Phys Lett*, 2009, **95**, 142106.
28. J. Kang, W. Liu, D. Sarkar, D. Jena and K. Banerjee, *Physical Review X*, 2014, **4**, 031005.
29. C. Chakraborty, R. Beams, K. M. Goodfellow, G. W. Wicks, L. Novotny and A. Nick Vamivakas, *Appl Phys Lett*, 2014, **105**, 241114.
30. X. Song, J. Hu and H. Zeng, *Journal of Materials Chemistry C*, 2013, **1**, 2952-2969.
31. S. Zhang, Z. Yan, Y. Li, Z. Chen and H. Zeng, *Angewandte Chemie*, 2015, **54**, 3112-3115.

### Figure Captions

**Figure 1. Characterizations of the PLD-grown WS<sub>2</sub> film.** (a) Digital photographs of a large-area multilayer WS<sub>2</sub> film on a 1×1 cm<sup>2</sup> Si substrate with 300 nm oxide layer. (b) SEM image, scale bar: 300 nm. (c) AFM surface topography image. (d) 2θ-ω X-ray diffraction pattern. (e) Raman spectroscopy with the 514 nm excitation laser.

**Figure 2. Optical and electrical properties of the PLD-grown WS<sub>2</sub> film.** (a) UV-VIS absorption spectrum. (b) Histogram of the mobility with the average value of 31 cm<sup>2</sup>V<sup>-1</sup>s<sup>-1</sup>. (c) Cross-section schematic diagram of a WS<sub>2</sub> photoresistor.

**Figure 3. Switching behavior of the WS<sub>2</sub> photoresistor under various illuminations.** The wavelengths of the incident light are (a) 370 nm, 110 mW/cm<sup>2</sup>, (b) 532 nm, 10 mW/cm<sup>2</sup>, (c) 635 nm, 55 mW/cm<sup>2</sup>, (d) 1064 nm, 42 mW/cm<sup>2</sup>. In all cases, the WS<sub>2</sub> photodetector yields significant photoresponse, demonstrating broadband photoresponse from ultraviolet to near-infrared.

**Figure 4. Photoresponse in the ambient environment.** (a) Temporal photoresponse of the WS<sub>2</sub> photoresistor. Power density: 18 mW/cm<sup>2</sup>. Source-drain bias: 0.5 V. (b) Power dependent photocurrent. Source-drain bias: 1.75 V. (c) Voltage dependent photocurrent and the corresponding responsivity. Power density: 18 mW/cm<sup>2</sup>. (d) Switching behavior over time. Source-drain bias: 0.6 V. Power density: 55 mW/cm<sup>2</sup>.

**Figure 5. Photoresponse in the vacuum environment.** (a) Switching behavior under cyclical illumination. Power density:  $18 \text{ mW/cm}^2$ . Source-drain bias: 0.5 V. (b) Power dependent photocurrent. Source-drain bias: 1.75 V. (c) Voltage dependent photocurrent and the corresponding responsivity. Power density:  $18 \text{ mW/cm}^2$ . (d) I-V curves in ambient and vacuum condition, the curves are vertically shifted for clarity. (e) Temporal photoresponse of the  $\text{WS}_2$  photoresistor. Power density:  $18 \text{ mW/cm}^2$ . Source-drain bias: 0.5 V. (f) Schematic illustration for the absorption and desorption process of an  $\text{O}_2$  molecular.

Figure 1

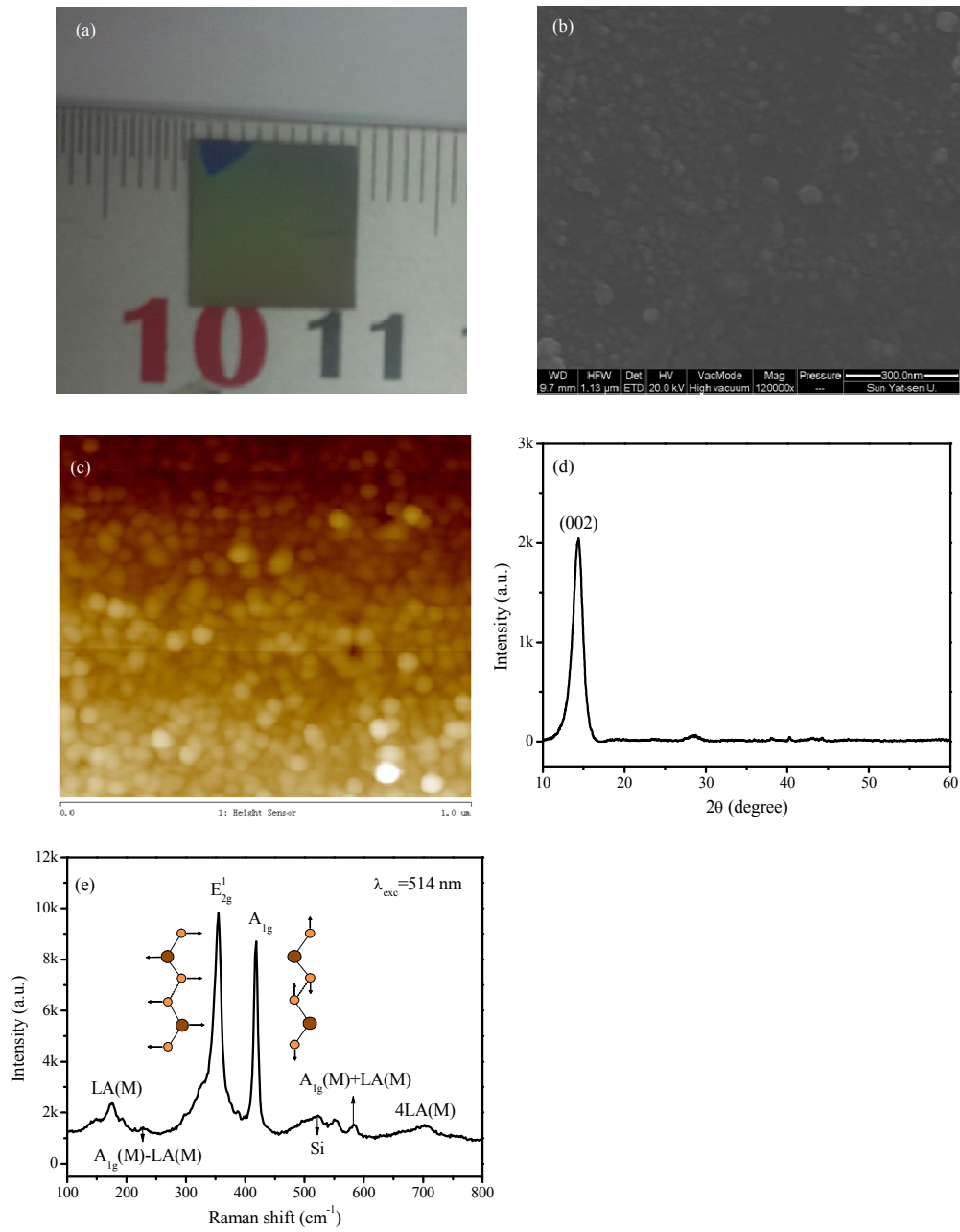


Figure 2

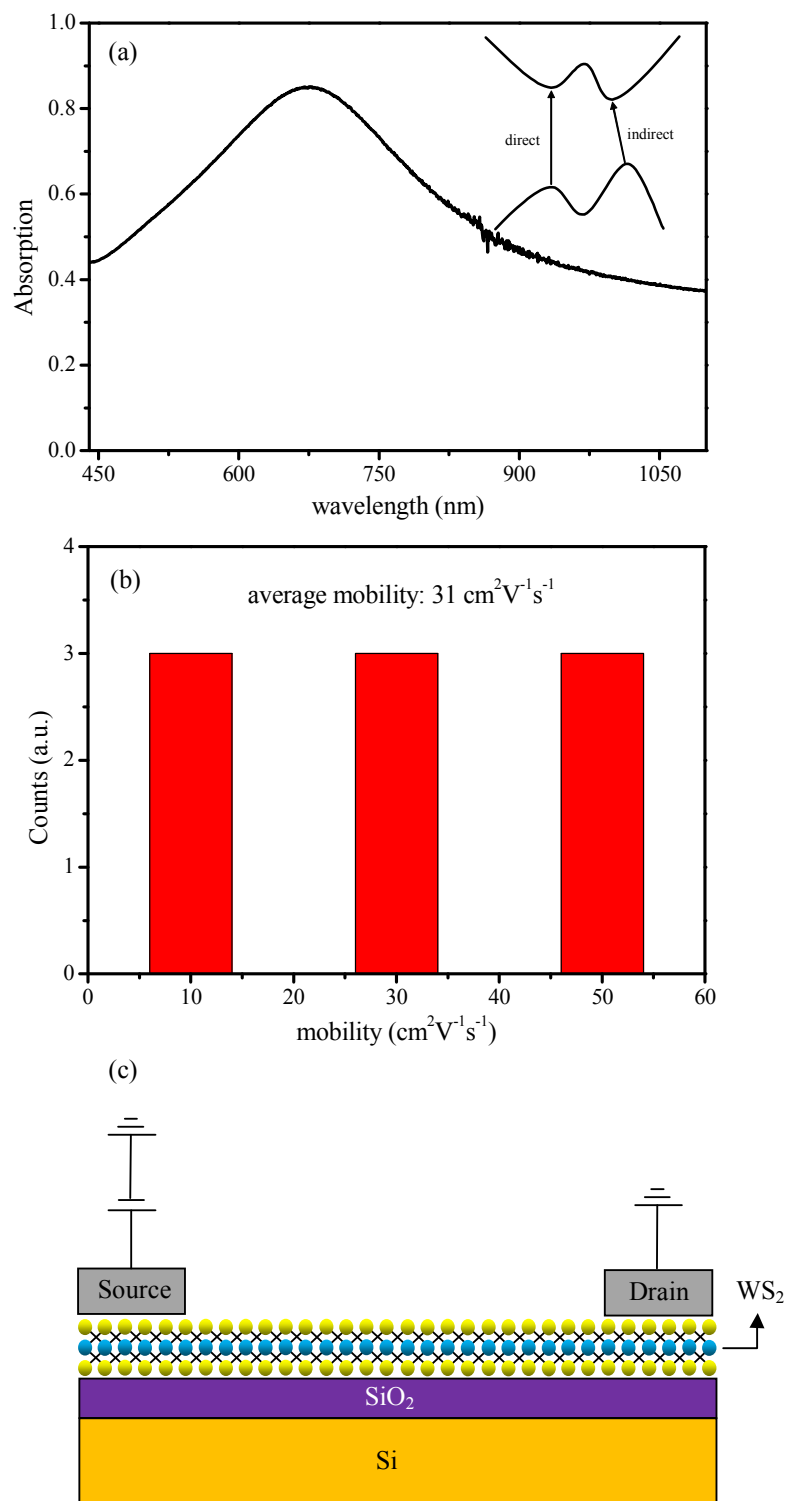


Figure 3

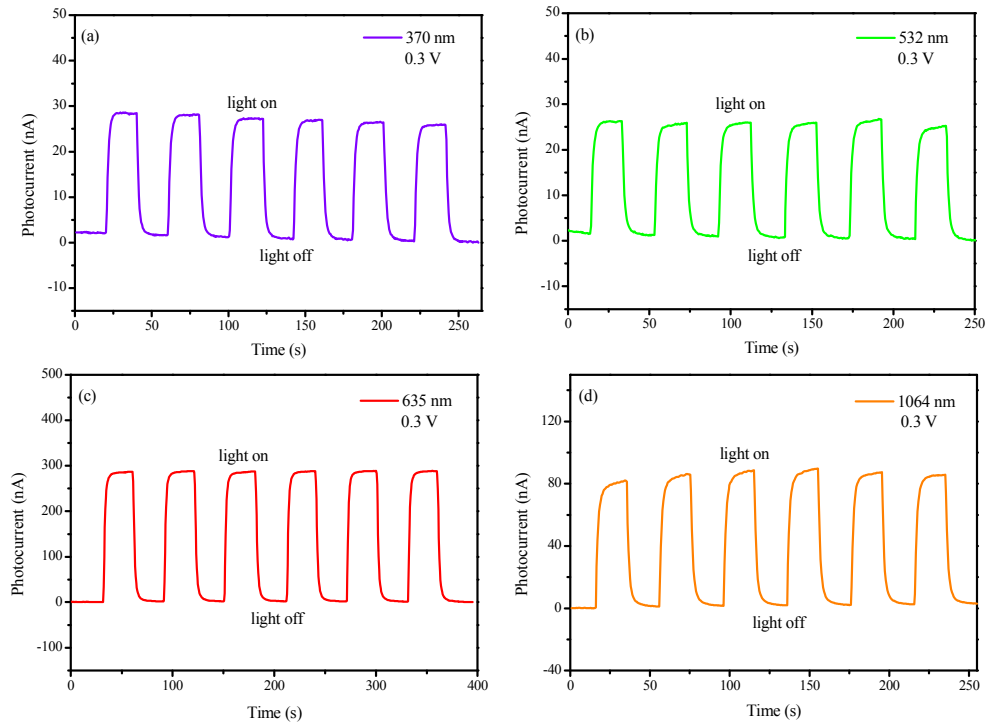


Figure 4

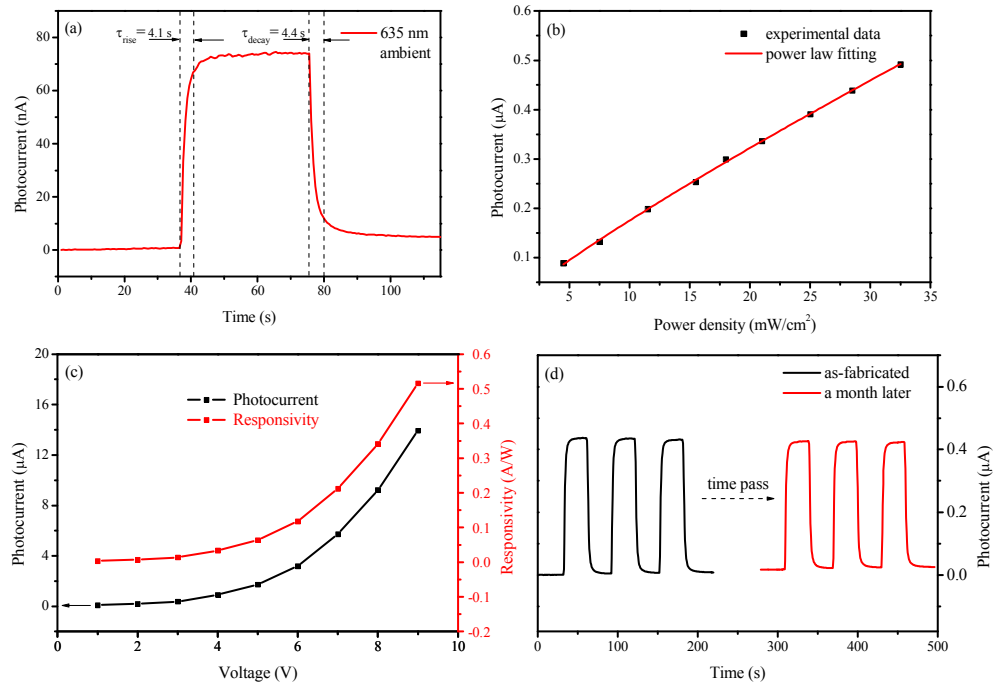


Figure 5

